Magnetic properties of Ba_2HoSbO_6 with a frustrated lattice geometry

S. Calder,[1,*] X. Ke,[2,†] F. Bert,[3,‡] A. Amato,[4] C. Baines,[4] C. Carboni,[5] R. J. Cava,[6] A. Daoud-Aladine,[7] P. Deen,[8] T. Fennell,[8] A. D. Hillier,[7] H. Karunadasa,[6,§] J. W. Taylor,[7] P. Mendels,[3] P. Schiffer,[2] and S. T. Bramwell[1]

[1]*London Centre for Nanotechnology, University College London, 17-19 Gordon Street, London WC1H 0AH, United Kingdom*

[2]*Department of Physics and Materials Research Institute, Pennsylvania State University, University Park, Pennsylvania 16802, USA*

[3]*Laboratoire de Physique des Solides, Université Paris-Sud XI, UMR CNRS 8502, 91 405 Orsay, France*

[4]*Paul Scherrer Institute, CH-5232 Villigen, Switzerland*

[5]*Department of Physics, Sultan Qaboos University, Al Khod, Sultanate of Oman*

[6]*Department of Chemistry and Princeton Materials Institute, Princeton University, Princeton, New Jersey 08540, USA*

[7]*ISIS Facility, Rutherford Appleton Laboratory, Chilton, Didcot, Oxfordshire OX11 0QX, United Kingdom*

[8]*Institut Laue-Langevin, 6 rue Jules Horowitz, BP 156, 38042 Grenoble Cedex 9, France*

(Received 8 December 2009; revised manuscript received 28 January 2010; published 23 February 2010)

The study of geometrically frustrated magnets with unusual crystal field ground states offers the possibility of discovering new aspects of the physics of cooperative paramagnetic states. In the rare-earth double perovskite Ba_2HoSbO_6 the Ho^{3+} ions occupy a face-centered cubic lattice, which frustrates near-neighbor antiferromagnetic coupling. We present a systematic experimental study of the system using dc magnetization, heat capacity, muon-spin relaxation, inelastic neutron scattering, neutron powder diffraction, and neutron polarization analysis. The bulk measurements at first point to spin liquid behavior, but the microscopic measurements indicate that this system is an example of a "nonmagnetic doublet" crystal field ground state, with low-lying excited states. Our measurements are interpreted using crystal field theory of Ho^{3+}, including hyperfine coupling. We find that exchange and dipolar coupling are weak in this particular system and that the "mock spin liquid" behavior in fact reflects the unusual properties of the nonmagnetic doublet.

DOI: 10.1103/PhysRevB.81.064425 PACS number(s): 75.10.Dg, 75.50.−y, 61.05.fg, 75.20.−g

I. INTRODUCTION

Geometrical magnetic frustration, the competition between spin-spin interactions, can lead to a variety of exotic low-temperature spin states. These include spin liquid and spin ice,[1–3] which are typically observed in materials based on corner-sharing units, such as the pyrochlore or kagomé lattices. The face-centered cubic (fcc) lattice is another geometry containing triangular or tetrahedral units and is also one of the simplest geometries on which atoms can be arranged. It is most commonly drawn to emphasize the cubic symmetry but can equivalently be represented as an edge-sharing tetrahedral structure with each site having 12 nearest neighbors (Fig. 1). Spins on an fcc lattice with nearest-neighbor antiferromagnetic interactions are therefore frustrated, with an infinite degeneracy of ground states.[4] For classical spins, the ground-state degeneracy is thought to be lifted by thermal fluctuations,[5] leading to a first-order phase transition at finite temperature.[6,7] For Heisenberg spins with nearest-neighbor coupling only, quantum fluctuations of the transverse spin component may however destabilize long-range order in favor of a spin liquid state.[8]

Despite the frustration associated with the fcc structure, no experimental examples of spin liquid states resulting from such frustration have yet been found. This is consistent with Maxwellian counting arguments, which predict an overconstraint of the spin degrees of freedom by the relatively large number of nearest neighbors.[1] Materials with the ordered double perovskite structure ($A_2BB'O_6$) have ions on the B and B' sites which form two independent interpenetrating fcc sublattices. Long-range magnetic ordering has been observed in compounds with transition metal ions (M=Co,Ni,Mn) occupying the B sites,[9–12] and spin glass behavior has also been reported (M=Re and Fe).[13–16] Double perovskites with magnetic rare-earth ions, however, have so far revealed no transition to long-ranged order or spin glass freezing down to 2 K, suggesting the possibility of a spin liquid ground state.[17–19]

A crucial factor in the study of the magnetic properties of rare-earth salts is the crystalline electric field (CEF) at the lanthanide site, which determines the electronic states of the single rare-earth ion. For example, in the case of the elpasolite series A_2BLnX_6 (Refs. 20–26) (A,B=Li, Na, K, Rb, and Cs; Ln is a lanthanide; X=F,Cl), which also contains an fcc lattice of rare-earth ions, CEF effects generally dominate those arising from magnetic coupling. For non-Kramers ions the materials behave as Van Vleck paramagnets with a nonmagnetic ground state, while for Kramers ions, the systems order at low temperature. Calculations based on crystal field theory gave reasonable fits to the measured magnetic susceptibility data[20–22] or optical spectral,[24,25] indicating that the magnetic behavior is well explained by a model of uncoupled ions (single-ion model).

Crystal-field interactions offer an interesting way of modifying the physics of basic models of magnetic frustration, as

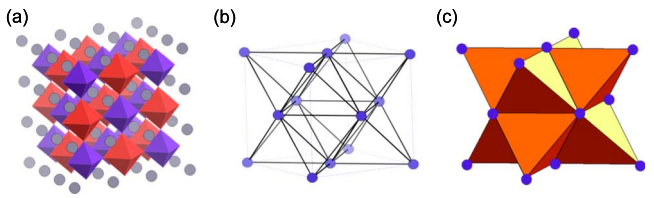

FIG. 1. (Color online) (a) The crystal structure of double perovskite Ba_2HoSbO_6. Spheres are Ba atoms and the two octahedra units shown represent HoO_6 and SbO_6. (b) The fcc-ordered Ho sublattice of double perovskite. (c) The arrangement of edge-sharing Ho tetrahedra in double perovskite.

has been amply demonstrated in the case of the rare-earth pyrochlores.[27,28] In the present context, a "nonmagnetic doublet" or Γ_3 CEF ground state would raise the possibility of a competition between an exchange-induced spin liquid (cooperative paramagnetic) phase and a phase with vanishing magnetic moment. Recent work by Goremychkin *et al.*[29] and by Molavian *et al.*[30] has emphasized how virtual crystal field excitations can lead to nontrivial effective interactions in frustrated systems. At an experimental level the Γ_3 ground state is known to play a role in nonmagnetic heavy-fermion behavior[31] and the phenomenon of enhanced nuclear magnetism.[32] Thus a careful study of model frustrated systems with Γ_3 ground states would seem to be worthwhile.

In this paper, we examine the low-temperature properties of a rare-earth double perovskite, Ba_2HoSbO_6, in which the Ho^{3+} ions occupy an fcc lattice (Fig. 1), through a combination of measurements of magnetic susceptibility, heat capacity, muon-spin relaxation (μSR), inelastic neutron scattering, neutron powder diffraction and polarized neutron scattering. We find no magnetic phase transition down to 20 mK, but persistent muon relaxation, a result that immediately suggests a spin liquid or cooperative paramagnetic low-temperature state. However we also establish that Ho^{3+} has a nonmagnetic CEF ground state. The Γ_3 single-ion CEF ground state of the Ho^{3+} ions is confirmed by a detailed analysis of the CEF scheme based on inelastic neutron scattering. The adoption of a model of uncoupled ions leads to calculated susceptibility and heat capacity which are in good agreement with the experimental measurements, suggesting that the CEF dominates any exchange or dipolar coupling in this system. The low-temperature μSR data are analyzed in terms of "enhanced nuclear magnetism," a specific feature of nonmagnetic ground-state ion with a Van Vleck susceptibility. These data demonstrate that single-ion physics can mimic many of the signatures of the canonical collective behavior of a spin liquid state, and the existence of such a "mock spin liquid" offers insight into the possible complexity associated with the combination of geometrical frustration and unusual crystal field structures.

II. EXPERIMENTAL METHODS

Polycrystalline samples of Ba_2HoSbO_6 were prepared as described elsewhere[17] using standard solid-state synthesis techniques. Room-temperature powder neutron-diffraction data confirmed all samples to be single-phase double perovskites, and a detailed structural analysis of the same batch of these materials has been described previously.[17] dc magnetization (M) was measured with a Quantum Design superconducting interference device magnetometer, and heat capacity (C) with a Quantum Design physical property measurement system cryostat equipped with the ^{3}He option, using a standard semiadiabatic heat-pulse technique. The μSR measurements were conducted at ISIS for the temperature range of 1.3–300 K and at PSI for the temperature range of 0.020–10 K. Powder neutron-diffraction measurements were carried out at the ISIS pulsed neutron source using the high-intensity and high-resolution diffractometer GEM between 20 and 1.5 K. XYZ neutron polarization analysis was performed on the D7 diffractometer at the ILL for the temperature range 0.06–5 K and an inelastic neutron-scattering experiment was performed at ISIS using the MARI spectrometer between ambient temperature and 5 K.

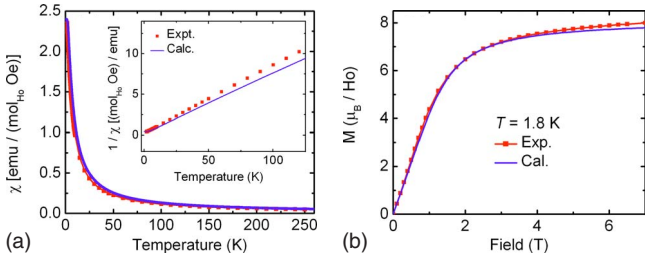

FIG. 2. (Color online) (a) dc magnetic susceptibility (M/H) as a function of temperature in a 100 Oe applied field (FC and ZFC results are identical); Inset shows the low-temperature inverse dc susceptibility. (b) The magnetic field dependence of the magnetization M at $T=1.8$ K for Ba_2HoSbO_6. Red and blue curves represent experimental and calculated data, respectively. See Sec. IV B for an explanation of the calculations.

III. EXPERIMENTAL RESULTS

A. dc magnetic susceptibility measurements

As shown in Fig. 2(a), field-cooled (FC) and zero-field-cooled (ZFC) measurements of the temperature dependence of the magnetization (M) of both samples indicate no anomalies corresponding to long-range ordering or spin glass freezing down to $T=1.8$ K. Fits to the Curie-Weiss expression over the range $T\sim250$ K to $T\sim100$ K give a single-ion moment of $10.0\mu_B$/Ho derived from the fitted Curie constant, which is close to the expected free-ion value of $10.6\mu_B$/Ho and consistent with a previous study.[17] At first sight there is evidence of antiferromagnetic exchange, as the fitted Curie-Weiss temperature is $\theta\approx-7.7$ K and the magnetization at $T=1.8$ K, [Fig. 2(b)], does not saturate even in a $\mu_0H=7$ T applied field.

B. Heat-capacity measurements

For the heat-capacity measurements, samples were pressed with silver powder into pellets at room temperature to facilitate thermal equilibration. In Fig. 3(a) we plot the temperature-dependent heat capacity of Ba_2HoSbO_6 at zero magnetic field after the silver and the sample holder background subtraction. In order to extract the magnetic heat capacity $C_{mag}(T)$, we prepared an isostructural nonmagnetic analog, Ba_2LaSbO_6, to estimate the lattice contribution. The dash-dotted curve, also shown in Fig. 3(a), represents the scaled heat-capacity data of Ba_2LaSbO_6. The resulting heat capacity after subtraction of the lattice contribution is shown in Fig. 3(b). The absence of a sharp peak in $C_{mag}(T)$ again indicates that there is no phase transition to long-range magnetic ordering. Instead there is a broad peak at $T\sim4$ K.

The most striking feature seen in Fig. 3(b) is the absence of a nuclear Schottky anomaly, which dominates the low-temperature heat capacity of many holmium compounds. That Schottky anomaly originates from the splitting of the

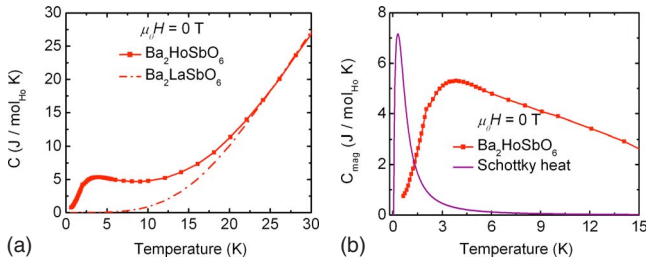

FIG. 3. (Color online) (a) Zero-field heat capacity for Ba_2HoSbO_6 as a function of temperature. The dashed-dotted curves are the scaled heat capacity of nonmagnetic Ba_2LaSbO_6. (b) Magnetic heat capacity of Ba_2HoSbO_6 after lattice subtraction at $\mu_0H=0$ T. The solid purple curve represents the Schottky heat capacity that is found in certain holmium compounds (see text) (Ref. 33).

nuclear-spin levels in the presence of a quasistatic magnetic field created by holmium electronic moments, i.e., the hyperfine interaction. For comparison, we show the expected nuclear Schottky contribution based on the low-temperature heat-capacity data for holmium metal[33] and the holmium spin ices.[34,35] The observed absence of the Schottky anomaly in the double perovskites suggests that the nuclear spins are not subjected to a static magnetic field from the electronic spins. This indicates that any electronic spin fluctuations occur on a time scale faster than the nuclear-spin relaxation time so that the average magnetic field from the electronic moments is close to zero.

To further probe the low-temperature behavior of this material, we measured the heat capacity in the presence of an applied magnetic field, as shown in Fig. 4(a) where we plot $C_{mag}(T)$ measured in different applied magnetic fields. The broad peak in the heat capacity develops at higher temperature in an applied field. An interesting feature of the data is

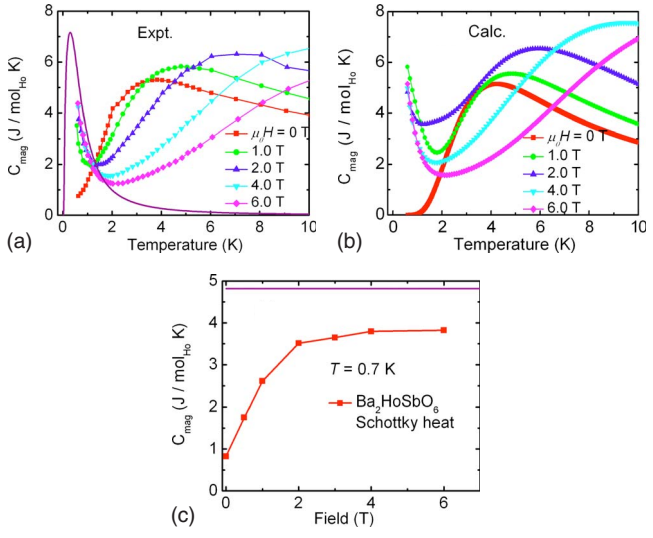

FIG. 4. (Color online) (a) Temperature dependence of heat capacity after phonon subtraction in different applied fields for Ba_2HoSbO_6 and (b) the corresponding calculated heat-capacity data as described in Sec. IV C. (c) Heat capacity of Ba_2HoSbO_6 as a function of applied magnetic field at $T=0.7$ K. The purple line (line below 5 J/mol_{Ho}K) represents the expected Schottky heat-capacity value of holmium at this temperature.

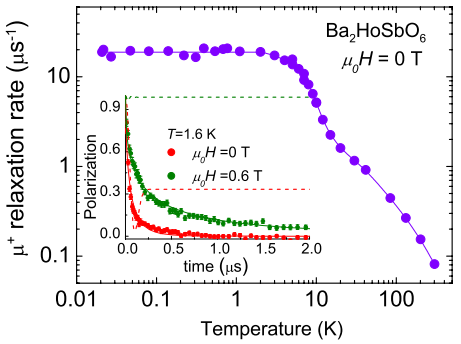

FIG. 5. (Color online) Muon relaxation rate, λ, as a function of temperature for Ba_2HoSbO_6. Inset: muon polarization decay at 1.6 K in zero field and $\mu_0H=0.6$ T. The solid curves are fit to stretched exponential functions. The dashed lines are Kubo-Toyabe relaxation curves, expected in the case of a frozen, fully disordered, ground state with a 0.02 T internal field distribution width, chosen to reproduce the fast initial relaxation in zero field. Note the characteristic 1/3 polarization recovery at long time, which is not observed in the data. Note also that applying a $\mu_0H=0.6$ T field in this static scenario should completely suppress the relaxation.

that C_{mag} increases dramatically at the lowest temperatures in the presence of a strong applied field. We attribute this increase to the emergence of the nuclear Schottky anomaly as holmium electronic moments become polarized along the field direction and produce a static mean field to which the nuclear spins are subjected. Figure 4(c) shows the field dependence of the heat capacity at $T=0.7$ K, which increases quickly with increasing magnetic field, and is close to saturation at around $\mu_0H=3$ T, reflecting the behavior of the sample magnetization. The saturated heat capacity is smaller than the calculated value for holmium metal as indicated by the solid purple line, which might be attributable to the unsaturated holmium moments at this field.

C. μSR measurements

We have also performed μSR measurements that extended our low-temperature range down to 20 mK. The inset to Fig. 5(a) shows the time dependence of the muon polarization in Ba_2HoSbO_6 at low temperature in zero field and with a $\mu_0H=0.6$ T field, applied along the beam polarization. The zero-field polarization shows a fast relaxation and no spontaneous oscillations that would be characteristic of long-range magnetic order. In the case of a static state with partial or full disorder, the spontaneous oscillations may be smeared out, but one would expect (i) a polarization value equal to 1/3 in the long time limit due to the powder average of the internal field with respect to the muon initial polarization and (ii) an absence of relaxation in an applied field of $\mu_0H=0.6$ T, much larger than the ~0.02 T static field distribution width needed to explain the fast initial relaxation.[36,37] The absence of both these signatures suggests that the electronic moments of Ho ions produce no static magnetic field in this material so that we can safely discard any magnetic phase transition in Ba_2HoSbO_6 down to 21 mK.

In the fast fluctuation limit, an exponential relaxation of the muon polarization is expected with the exponent[37]

$$\lambda = \frac{2\gamma_\mu^2 \mu_0^2 H_\mu^2 \nu}{\gamma_\mu^2 \mu_0^2 H^2 + \nu^2}, \quad (1)$$

where $\gamma_\mu/2\pi = 135.5$ MHz/T is the muon gyromagnetic ratio, H_μ is the characteristic width of the fluctuating field distribution at the muon site, ν is the fluctuation rate and H the applied field, if any. The time-dependent polarization in Ba_2HoSbO_6 in zero applied field was fitted to a stretched exponential $\exp[-(\lambda t)^\beta]$ with $\beta = 0.75 \pm 0.1$, likely reflecting a distribution of relaxation times. The thermal dependence of the characteristic muon relaxation rate λ is plotted in the main panel of Fig. 5 and indicates a slowing down of the magnetic fluctuations from 300 K down to 5 K, where the fluctuation rate saturates and remains constant down to 20 mK. Marked changes in the muon relaxation rate at about 15 and 5 K are noticeable and likely reflect the Ho^{3+} CEF level scheme through changes in the field H_μ at the muon site.

From the fits of the muon polarization plotted in the inset of Fig. 5, and using Eq. (1) for $\mu_0 H = 0$ T and $\mu_0 H = 0.6$ T, we estimate that on the low-temperature dynamical plateau ($T < 5$ K), $\nu \sim 300$ MHz and $\mu_0 H_\mu \sim 0.07$ T. This latter value of the field at the muon site is surprisingly small since if one makes the usual assumption that muons (being positively charged) stop next to the oxygen O^{2-} ion, and that the Ho^{3+} moment is about $10\mu_B$, $\mu_0 H_\mu$ is expected to be on the order of 1 T. This point will be addressed later in the discussion after the determination of the Ho^{3+} CEF parameters.

D. Neutron-scattering experiments

Neutron powder-diffraction measurements were carried out using the GEM diffractometer at ISIS and the polarized neutron diffractometer D7 at the ILL in zero applied field. The results collected at 20 and 1.5 K from GEM were refined using GSAS starting from the lattice parameters reported in the literature.[17] With these parameters the refined crystallographic model gave good agreement with the experimental data indicating that the crystal structure of Ba_2HoSbO_6 remains cubic between room temperature and at least 1.5 K. There is no appearance of additional intensity, Bragg peaks, or diffuse scattering in the diffraction pattern between 20 and 1.5 K indicating the absence of magnetic order.

To investigate the low-temperature magnetic properties of Ba_2HoSbO_6 further, neutron polarization analysis was carried out on D7 down to 60 mK. So-called "xyz" analysis allows the complete separation of the various nuclear and magnetic contributions to the scattering that combine to give the total scattering observed in standard diffraction such as that performed on GEM.[38] This technique is therefore extremely powerful in obtaining unequivocal magnetic information, as the coherent magnetic scattering arising from electronic magnetic moments can be isolated (henceforth we simply call this "the magnetic scattering"). Starting from empirical analytical formulas and using relevant coefficients[39] the magnetic form factor for Ho^{3+} was compared to the magnetic neutron scattering using a least-squares fitting package. As shown in Fig. 6, the magnetic scattering closely follows the form factor squared of Ho^{3+}, with no variation between 60 mK and 5 K. This again confirms that there is no magnetic phase transition in this temperature range and additionally rules out any significant spin-spin correlation which would necessarily lead to departures from the observed form.

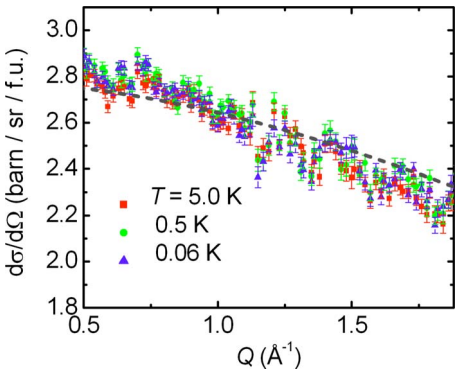

FIG. 6. (Color online) Magnetic component of Ba_2HoSbO_6 from the xyz-polarized neutron diffractometer D7 at the ILL. No magnetic order is present and the $|Q|$-dependent scattering fits the form factor for Ho^{3+} between 5 and 0.06 K, shown by the dashed line in the plot.

To investigate the crystalline electric field, we performed inelastic neutron spectroscopy measurements on Ba_2HoSbO_6 using the MARI spectrometer at ISIS. In the investigation of magnetic frustrated systems, obtaining crystal field parameters and finding the associated crystal field level scheme have been proven to be extremely useful in explaining observed properties and ground states adopted.[28] Figure 7 shows the inelastic neutron data at $T = 5$ and 200 K with initial neutron energies of 8 and 60 meV. The implications of these results will be discussed below.

IV. ANALYSIS AND DISCUSSION

As described above, there is no magnetic phase transition in Ba_2HoSbO_6 down to 21 mK, and persistent dynamics re-

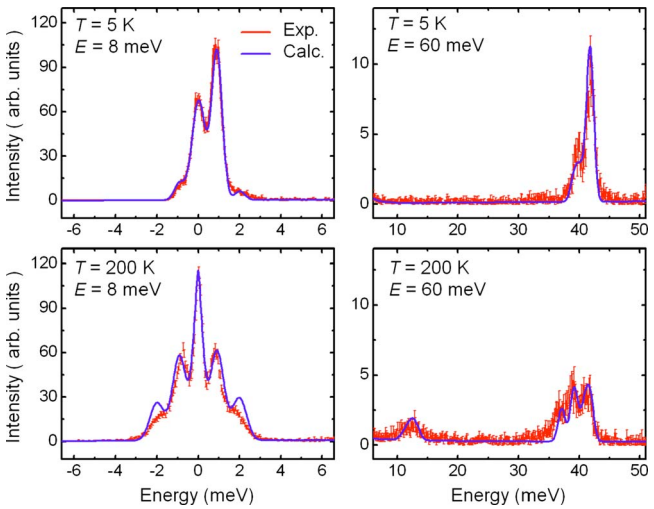

FIG. 7. (Color online) Inelastic neutron-scattering data (crosses) taken with the incident neutron energy $E_i = 8$ and 60 meV at $T = 5$ and 200 K. The solid curves are the best fit of the data using the FOCUS fitting package through ISIS.

vealed by μSR, possibly suggesting a spin liquid state with a surprisingly low value of the fluctuating field. However cooperative paramagnetism (signaled by finite spin correlations) is ruled out by the neutron-scattering measurements. Thus Ba_2HoSbO_6 does not afford another example of the spin liquid state that has been reported in other geometrically frustrated systems.[40–47] In order to clarify the nature of the ground state of Ba_2HoSbO_6, we now present our analysis of the crystal field level scheme of Ho^{3+}, based on the inelastic neutron-scattering measurements. As advertised, we find that the Ho^{3+} ions have a nonmagnetic ground state, which, combined with weak magnetic coupling, largely accounts for the bulk measurements presented above. Ba_2HoSbO_6 is thus a Van Vleck paramagnet with a nonmagnetic ground state, as has been observed in fluoride and chloride-based double perovskites with integer value of total angular momentum of the rare-earth ions.[25]

A. Crystalline electric field

The crystal field Hamiltonian can be expressed as

$$H_{\mathrm{CEF}} = \sum_{nm} B_n^m O_n^m, \tag{2}$$

where O_n^m are Stevens' operators acting on the J angular momentum states and B_n^m are the CEF parameters.[48] The symmetry at the site of the rare-earth ion under investigation determines which of the terms in H_{CEF} are nonzero. For the site of cubic symmetry, $m3m$, of the Ho^{3+} ions in Ba_2HoSbO_6 there are only four terms in the crystal field Hamiltonian. Furthermore, there is a simple relation between the two fourth-order terms and the two sixth-order terms. Therefore only two parameters B_4 and B_6 are required to describe the CEF. H_{CEF} is written as follows:

$$H_{\mathrm{CEF}} = B_4^0[O_4^0 + 5O_4^4] + B_6^0[O_6^0 - 21O_6^4]. \tag{3}$$

To determine the crystal field parameters from neutron spectroscopy it is convenient to make use of the results of Lea, Leask, and Wolf (LLW) (Ref. 49) wherein the normalized eigenvectors and eigenvalues for all integer and half integer J values between 2 and 8 were tabulated using all possible values of the ratio between the two crystal field parameters. In this way the problem of finding values for the crystal field parameters in cubic symmetry is reduced to a one-dimensional problem, without approximation.

They achieve this by rewriting Eq. (3) in the following form:

$$H_{\mathrm{CEF}} = B_4^0 F(4)\frac{O_4^0 + 5O_4^4}{F(4)} + B_6^0 F(6)\frac{O_6^0 - 21O_6^4}{F(6)}, \tag{4}$$

where $F(4)$ and $F(6)$ are constant factors for a particular J. To cover all the possible values of the ratio between B_4 and B_6 LLW set,

$$B_4^0 F(4) = WxB_6^0 F(6) = W(1 - |x|), \tag{5}$$

where $-1 \leq x \leq 1$ and W is introduced in these equations as a scale factor between $-\infty \leq W \leq \infty$ for the crystal field energy levels. The CEF parameters can then be found by scanning

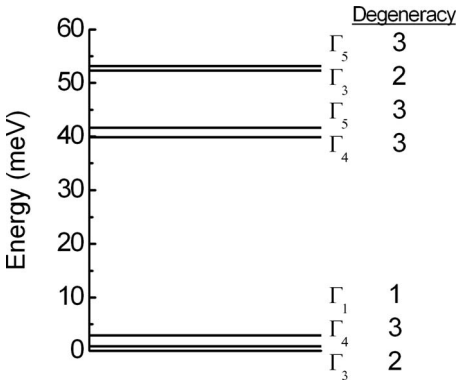

FIG. 8. Calculated crystal field energy levels for Ho^{3+} in Ba_2HoSbO_6.

for possible values which match the pattern of the peaks from neutron spectroscopy by varying x, and then applying an appropriate energy scaling value W, where these values are entirely equivalent to the B_4 and B_6 parameters. All the possible x positions from the LLW plots that could be realistically matched to the spectra of peaks were used to find and verify a fit to the data. Ultimately it was found that only one region, around $x=0.76$, allowed a close fit to peak position and intensity along with the peak variation with temperature. Using the least-squared fitting package FOCUS,[50] we find that the $x=0.761$ and $W=-0.0504$ meV provides the best fit to the inelastic neutron-scattering data for all temperatures measured between 300 and 5 K (Fig. 7), as shown by the solid curves.

The CEF parameters for Ho^{3+} in Ba_2HoSbO_6 are therefore found to be

$$B_4^0 = -0.123 \times 10^{-2} \text{ meV},$$

$$B_6^0 = -0.167 \times 10^{-5} \text{ meV}$$

with an error of $\pm 0.007 \times 10^{-2}$ and $\pm 0.007 \times 10^{-5}$ on B_4^0 and B_6^0, respectively.

The CEF energy-level scheme is shown in Fig. 8. The lowest-lying energy level for Ba_2HoSbO_6 is in Bethe's notation Γ_3,[51] which is a nonmagnetic doublet. The Γ_3 doublet is nonmagnetic since both degenerate eigenstates [$\Gamma_3(a)$ and $\Gamma_3(b)$] have symmetric wave functions with no matching m_J states between the wave functions. For Ho^{3+} in Ba_2HoSbO_6 $\Gamma_3(a) = 0.574|-8.0\rangle - 0.229|-4.0\rangle - 0.486|0.0\rangle - 0.229|4.0\rangle + 0.574|8.0\rangle$ and $\Gamma_3(b) = 0.045|-6.0\rangle + 0.706|-2.0\rangle + 0.706|2.0\rangle + 0.045|6.0\rangle$. Hence the magnetic moment, given by the expectation $|\langle\Gamma_i|J_z|\Gamma_i\rangle|$, is zero.

This supports the lack of magnetic ordering as described in the experimental section and again excludes cooperative paramagnetic behavior. It is, however, important to note that the presence of a nonmagnetic ground state does not necessarily preclude magnetic effects and even the development of magnetic order in the system since this can occur through mixing of higher crystal field levels into the ground state by the magnetic exchange interaction. The first two excited levels are a triplet and a singlet, which are magnetic and nonmagnetic, respectively.

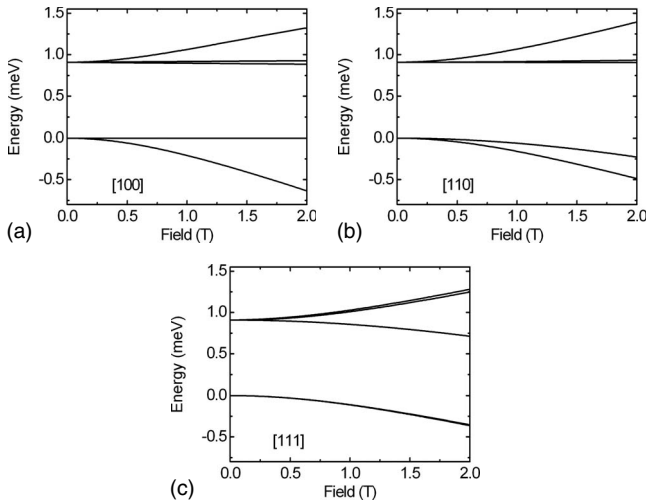

FIG. 9. Splitting of the twofold and threefold degeneracy of the ground state and first excited crystal field energy levels due to an applied field as calculated using Eq. (6) described in the text.

An applied magnetic field lifts the degeneracy of the crystal field levels and causes admixture of the states. This admixture leads to the possibility of a crossover of the energy levels which changes the nature of the ground state.[52–55] Because the magnetic interaction due to the applied field is of the same order as the crystal field interaction the ion is described by the combined Hamiltonian

$$H_F = H_{\mathrm{CEF}} - g_J \mu_B \mathbf{H} \cdot \mathbf{J}, \tag{6}$$

where g_J is the Landé factor, μ_B the Bohr magneton, and $\mathbf{H}$ the applied magnetic field. The calculated field dependence of the two lowest-energy levels of Ho^{3+} in Ba_2HoSbO_6 is shown in Fig. 9. It is clear that there is no level crossing between the doublet levels and triplet levels. The validity of this prediction is currently being tested in field-dependent measurements.

B. Calculation of susceptibility and magnetization

Using the wave functions and energies tabulated by LLW for compounds with cubic symmetry, one can calculate the magnetic susceptibility using the Van Vleck formula,[56]

$$\chi = \frac{N g_J^2 \mu_B^2}{Q k_B T}\left[\sum_i |\langle \Gamma_i | J_z | \Gamma_i \rangle|^2 \exp\left(\frac{-E_i}{k_B T}\right)\right] + \frac{2 N g_J^2 \mu_B^2}{Q}\left[\sum_{i,j} \frac{|\langle \Gamma_i | J_z | \Gamma_j \rangle|^2}{E_j - E_i} \exp\left(\frac{-E_i}{k_B T}\right)\right] \tag{7}$$

and the zero-field partition function,

$$Q = \sum_i g_i \exp\left(\frac{-E_i}{k_B T}\right), \tag{8}$$

where N is Avogadro's number, J_z the z component of the total angular momentum J. $|\Gamma_i\rangle$ are the eigenstates of the Hamiltonian which has energy given by E_i where the number of identical terms are taken into account by introducing a degeneracy factor.

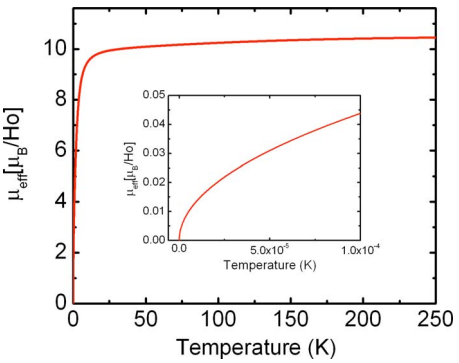

FIG. 10. (Color online) Effective moment calculated from the Van Vleck susceptibility. Inset is the expanded view of the low-temperature region.

The calculated susceptibility for Ba_2HoSbO_6 is shown by the solid curve in Fig. 2(a), which is in good agreement with experimental data. This confirms the validity of the crystal field parameters discussed above. Note that the saturation of the susceptibility to a finite value as $T \to 0$ reflects the second (Van Vleck) term in Eq. (7). It should be emphasized that a finite susceptibility at $T=0$ is not inconsistent with zero moment. Thus χ represents the moment induced by a weak field, and is related to the variance of the zero-field moment fluctuations by $\sigma^2 \propto \chi T$, which disappears at $T=0$.

It is interesting to note that, although the derived magnetic moment from the Curie-Weiss fit shown in Fig. 2(a) is close to the free-ion moment for Ho^{3+}, this does not preclude a nonmagnetic ground state. Figure 10 shows the calculated effective moment using the identity $\mu_{eff} = \sqrt{\chi k_B T / N}$ (this quantity should not be confused with the moment derived from the Curie constant, described above). It is clearly seen that the effective moment remains close to the free-ion moment of $10.6\mu_B$ down to around 10 K, which corresponds to the energy between the nonmagnetic ground state and first excited magnetic crystal field level. Then there is a sharp drop off due to depopulation of excited states due to thermal excitations being ever more statistically prohibited until the effective moment vanishes at 0 K, indicating that there is no induced moment effect in zero field. Experimental confirmation of this would confirm that there is no mixing of levels due to exchange interactions. The susceptibility itself saturates to a finite maximum value as the temperature approaches absolute zero, reflecting the quantum fluctuations of the magnetic moment about its zero mean value.

The large finite Van Vleck susceptibility is consistent with the form factor observed by neutron polarization analysis. According to the single-ion model, in the zero-temperature limit, the scattering should arise purely from the excitation (by neutron energy loss) of higher crystal field states, which is temperature independent.

The match between experiment and theory for the single-ion model thus largely rules out the possibility of there being any significant induced moment due to mixing of energy levels which can occur if the critical ratio of the effective exchange field to the crystal field is reached. The single-ion crystal field model used here can thus explain all the zero-field behavior described above. In order to put an upper

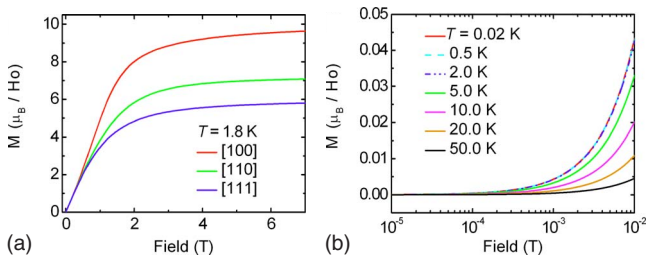

FIG. 11. (Color online) Calculated magnetization from CEF parameters for Ba_2HoSbO_6 at (a) 1.8 K for the field applied along the principal axes and (b) various temperatures for a field applied along [100] direction.

bound on the magnitude of any induced moment, it would be appropriate to extend the study of the bulk magnetic susceptibility down to very low temperature.

We now turn to the applied field measurements. The magnetization $M(\mu_0 H,T)$ is derived by adding the Zeeman term to the crystal field Hamiltonian [Eq. (6)] and is given by the following equation:[57]

$$M(\mu_0 H,T) = g_J \mu_B \frac{\sum_i \langle i|\mathbf{J}\cdot\hat{\mathbf{H}}|i\rangle \exp\left(\frac{-E_i(H)}{kT}\right)}{\sum_i \exp\left(\frac{-E_i(H)}{kT}\right)} \quad (9)$$

where $\hat{\mathbf{H}}$ is a unit vector of the applied magnetic field. Figure 11(a) shows the calculated isothermal curves at $T=1.8$ K with magnetic field applied along three principal axes. The magnetization is not saturated in $\mu_0 H$ fields up to 7 T with the calculated values depending on applied field directions. The result of the powder averaging magnetization is shown by the blue curve in Fig. 2(b), which is also in good agreement with the experimental data. Figure 11(b) shows the predicted results for a low field applied along the [100] direction. It is clear that for any finite field there is magnetization induced in the sample, even at low temperatures. This highlights the fact that even a small applied magnetic field will perturb the zero-field CEF scheme and result in an induced magnetic moment, although the ground state is nonmagnetic at zero applied field.

C. Calculation of specific heat

The solved crystal field Hamiltonian was used to calculate the magnetic heat capacity in zero and applied magnetic fields. The specific heat was calculated by first finding the eigenstates of the Hamiltonian in Eq. (6) and then adding the hyperfine interaction as a perturbation on these states. The hyperfine splitting of the states is described to first order by the effective nuclear-spin Hamiltonian[58]

$$H = h\left\{a_t I_z + P_t\left[I_z^2 - \frac{1}{3}I(I+1)\right]\right\}, \quad (10)$$

where I is the nuclear spin, a_t and P_t are, respectively, the dipolar and the quadrupolar hyperfine parameters. The z axis is chosen to be parallel to the total angular momentum J. For $^{165}Ho^{3+}$ ($I=7/2$ and $J=8$) there are 136 levels.

There are intraionic and extraionic contributions to the hyperfine parameters. Because of the strong hyperfine coupling in Ho^{3+}, the total dipolar hyperfine constant a_t is dominated by the dipolar intraionic term

$$a' = a_o\langle J_z\rangle, \quad (11)$$

where a_o is the dipolar hyperfine coupling constant and the expectation value $\langle J_z\rangle$ is calculated for each state under consideration. In the present case the extraionic contribution a'' is entirely due to the applied field; $a''=8.9$ MHz/T. The total dipolar parameter is the sum $a_t=(a'+a'')$. At a site of cubic symmetry there is no extraionic contribution to the quadrupolar parameter and there is just the intraionic part $P_t = P_0\langle 3J_z^2+J(J+1)\rangle/J(2J+1)$.

The contribution to the specific heat in an applied field at a given temperature T is then given by

$$C = \frac{k_B}{(k_B T)^2}\left[\sum_i E_i^2 P_i - \left(\sum_i E_i P_i\right)^2\right], \quad (12)$$

where the sum is carried out over the 136 energy levels E_i; here P_i is the population of the ith state.

The calculated contribution to the heat capacity at various applied magnetic fields averaged for the polycrystalline nature of the specimen is shown in Fig. 4(b). The data is in good agreement with the experimental results seen in Fig. 4(a). At zero fields there is no nuclear Schottky anomaly which indicates that there is no hyperfine splitting. The angular momentum of the Ho^{3+} ion is fully quenched ($\langle J_z\rangle=0$ and therefore $a_t=0$). This confirms that the ground state is nonmagnetic. The applied field induces a moment in the Ho^{3+} ion and the concomitant large hyperfine splitting of the states induces the Schottky anomaly in applied fields. We note that the induced magnetic moment on the Ho^{3+} ion is not saturated in fields up to $\mu_0 H=7$ T, which results in a lower value of the nuclear Schottky anomaly than the one observed in a compound where the holmium ion is fully polarized ($\langle J_z\rangle=8$). We mention in passing that as shown in Fig. 10(a) the calculated induced moment and therefore heat-capacity data strongly depend on the direction of the applied fields (data not shown). Measurements on single-crystal samples would be necessary to confirm this behavior.

D. μSR of the single-ion model

In the analysis of the low-temperature μSR data, we found a characteristic fluctuating field at the muon site $\mu_0 H_\mu \simeq 0.07$ T, too small to be due to the full electronic moment of Ho^{3+}. Another source of magnetism is of nuclear origin which usually leads to much smaller dipolar internal fields on the order of 1 G. However, in the special case of Van Vleck paramagnets, nuclear magnetism can be strongly enhanced through the magnetic hyperfine structure[59] and lead to unusually large internal field distribution at the muon site.[32] The ^{165}Ho hyperfine coupling constant $a=130.6$ mol/emu (Ref. 59) and the T-independent Van Vleck susceptibility of Ba_2HoSbO_6, $c=\chi=2.4$ emu/mol Ho, yield a strong enhancement factor of $(1+ac)$

$\simeq 310$. Therefore, for temperatures smaller than the first excited Γ_1 level energy 0.91 meV, the dipolar field $\simeq 2.8$ G at the muon (O^{2-}) site due to the 4.03 nuclear magnetons moment of a single $^{165}Ho^{3+}$ ion is enhanced to $\simeq 0.09$ T which compares favorably to our experimental determination $\mu_0 H_\mu \simeq 0.07$ T. Besides, from the observed fluctuation rate $\nu \simeq 300$ MHz at low temperature, we can estimate the nuclear interaction $J_{nuc}/k_B \approx \hbar\nu/k_B \approx 2$ mK. A rough calculation of the dipolar field at a Ho site created by a nearest-neighbor enhanced ^{165}Ho nuclear moment yields the energy scale of 3 mK so that the nuclear interaction J_{nuc} can be ascribed to enhanced nuclear dipole-dipole interaction. In conclusion we find that the μSR data can be understood consistently in terms of enhanced nuclear magnetism of the ^{165}Ho only with the assumption of a truly nonmagnetic ground state for the Ho^{3+} ion.

V. CONCLUSION

Our measurements establish that the Ba_2HoSbO_6 double perovskite with an fcc magnetic lattice is an example of a Van Vleck paramagnet with a nonmagnetic doublet ground state. As discussed above, the study of such a system is potentially interesting, as there must be a competition between a cooperative paramagnetic state and a nonmagnetic state. In Ba_2HoSbO_6, we find no magnetic phase transition down to very low temperature (20 mK). While either cooperative paramagnetism or nonmagnetic behavior would be consistent with these observations, neutron scattering shows that the single-ion CEF effect is dominant in this material. It would be of great interest to find an experimental system, perhaps a double perovskite, in which the competition between exchange and CEF is more evenly balanced. In this context, our investigation of Ba_2HoSbO_6 may serve as a useful benchmark.

ACKNOWLEDGMENTS

We acknowledge the financial support from NSF under Grant No. DMR-0701582, and from ANR grant "OxyFonda" under Grant No. NT05-4_41913. This research project has been supported by the European Commission under the Sixth Framework Programme through the Key Action: strengthening the European Research Area, Research Infrastructures under Contract No. RII3-CT-2003-505925.

*s.calder@ucl.ac.uk

†Present address: Neutron Scattering Science Division, Oak Ridge National Laboratory, Oak Ridge, Tennessee 37831, USA; kex1@ornl.gov

‡bert@lps.u-psud.fr

§Present address: Department of Chemistry, University of California–Berkeley, Berkeley, CA, USA.

[1] A. P. Ramirez, *Handbook of Magnetic Materials* (Elsevier, New York, 2001).
[2] R. Moessner, Can. J. Phys. **79**, 1283 (2001).
[3] S. T. Bramwell and M. J. P. Gingras, Science **294**, 1495 (2001).
[4] T. Oguchi, H. Nishimori, and Y. Taguchi, J. Phys. Soc. Jpn. **54**, 4494 (1985).
[5] C. L. Henley, J. Appl. Phys. **61**, 3962 (1987).
[6] H. T. Diep and H. Kawamura, Phys. Rev. B **40**, 7019 (1989).
[7] M. T. Heinilä and A. S. Oja, Phys. Rev. B **48**, 16514 (1993).
[8] E. Kuz'min, J. Exp. Theor. Phys. **96**, 129 (2003).
[9] D. Iwanaga, Y. Inaguma, and M. Itoh, Mater. Res. Bull. **35**, 449 (2000).
[10] A. Azad, S. Ivanov, S. Eriksson, J. Eriksen, H. Rundlof, R. Mathieu, and P. Svedlindh, Mater. Res. Bull. **36**, 2215 (2001).
[11] A. Muñoz, J. Alonso, M. Casais, M. Martinez-Lope, and M. Fernandez-Diaz, J. Phys.: Condens. Matter **14**, 3285 (2002).
[12] Jan-Willem G. Bos and J. P. Attfield, Phys. Rev. B **70**, 174434 (2004).
[13] R. Rodriguez, A. Fernandez, A. Isalgue, J. Rodriguez, A. Labarta, J. Tejada, and X. Obradors, J. Phys. C **18**, L401 (1985).
[14] P. Battle, T. Gibb, A. Herod, S. Kim, and P. Munns, J. Mater. Chem. **5**, 865 (1995).
[15] C. R. Wiebe, J. E. Greedan, G. M. Luke, and J. S. Gardner, Phys. Rev. B **65**, 144413 (2002).
[16] C. R. Wiebe, J. E. Greedan, P. P. Kyriakou, G. M. Luke, J. S. Gardner, A. Fukaya, I. M. Gat-Malureanu, P. L. Russo, A. T. Savici, and Y. J. Uemura, Phys. Rev. B **68**, 134410 (2003).
[17] H. Karunadasa, Q. Huang, B. G. Ueland, P. Schiffer, and R. J. Cava, Proc. Natl. Acad. Sci. U.S.A. **100**, 8097 (2003).
[18] K. Henmi, Y. Hinatsu, and N. Masaki, J. Solid State Chem. **148**, 353 (1999).
[19] Y. Kanaiwa, M. Wakeshima, and Y. Hinatsu, Mater. Res. Bull. **37**, 1825 (2002).
[20] E. Bucher, H. J. Guggenheim, K. Andres, G. W. Hull, and A. S. Cooper, Phys. Rev. B **10**, 2945 (1974).
[21] B. D. Dunlap and G. K. Shenoy, Phys. Rev. B **12**, 2716 (1975).
[22] C. Cheng and P. Dorain, J. Chem. Phys. **65**, 785 (1976).
[23] G. E. Fish, M. H. North, and H. J. Stapleton, J. Chem. Phys. **73**, 4807 (1980).
[24] J. P. Morley, T. R. Faulkner, F. S. Richardson, and R. W. Schwartz, J. Chem. Phys. **75**, 539 (1981).
[25] C. A. Morrison, R. P. Leavitt, and D. E. Wortman, J. Chem. Phys. **73**, 2580 (1980).
[26] E. Veenendaal, H. Brom, and W. Huiskamp, Physica B & C **121**, 1 (1983).
[27] M. J. P. Gingras, B. C. den Hertog, M. Faucher, J. S. Gardner, S. R. Dunsiger, L. J. Chang, B. D. Gaulin, N. P. Raju, and J. E. Greedan, Phys. Rev. B **62**, 6496 (2000).
[28] S. Rosenkranz, A. P. Ramirez, A. Hayashi, R. J. Cava, R. Siddharthan, and B. S. Shastry, J. Appl. Phys. **87**, 5914 (2000).
[29] E. A. Goremychkin, R. Osborn, B. D. Rainford, R. T. Macaluso, D. T. Adroja, and M. Koza, Nat. Phys. **4**, 766 (2008).
[30] H. R. Molavian, M. J. P. Gingras, and B. Canals, Phys. Rev. Lett. **98**, 157204 (2007).
[31] T. Kelley, W. Beyermann, R. Robinson, H. Nakotte, P. Canfield, and F. Trouw, Physica B **259-261**, 163 (1999).

[32] D. E. MacLaughlin, R. H. Heffner, G. J. Nieuwenhuys, P. C. Canfield, A. Amato, C. Baines, A. Schenck, G. M. Luke, Y. Fudamoto, and Y. J. Uemura, Phys. Rev. B **61**, 555 (2000).
[33] O. V. Lounasmaa, Phys. Rev. **128**, 1136 (1962).
[34] A. L. Cornelius and J. S. Gardner, Phys. Rev. B **64**, 060406(R) (2001).
[35] G. Lau, R. Freitas, B. Ueland, B. Muegge, E. Duncan, P. Schiffer, and R. Cava, Nat. Phys. **2**, 249 (2006).
[36] S. J. Blundell, Contemp. Phys. **40**, 175 (1999).
[37] R. S. Hayano, Y. J. Uemura, J. Imazato, N. Nishida, T. Yamazaki, and R. Kubo, Phys. Rev. B **20**, 850 (1979).
[38] J. R. Stewart, P. P. Deen, K. H. Andersen, H. Schober, J.-F. Barthélémy, J. M. Hillier, A. P. Murani, T. Hayes, and B. Lindenau, J. Appl. Crystallogr. **42**, 69 (2009).
[39] P. J. Brown, in *International Tables for Crystallography*, edited by A. J. C. Wilson, Volume C: Mathematical, Physical and Chemical Tables (Kluwer Academic Publishers, Dordecht, The Netherlands, 2004), Chap. 4.4.5.
[40] F. Bert, P. Mendels, A. Olariu, N. Blanchard, G. Collin, A. Amato, C. Baines, and A. D. Hillier, Phys. Rev. Lett. **97**, 117203 (2006).
[41] Y. J. Uemura, A. Keren, K. Kojima, L. P. Le, G. M. Luke, W. D. Wu, Y. Ajiro, T. Asano, Y. Kuriyama, M. Mekata, H. Kikuchi, and K. Kakurai, Phys. Rev. Lett. **73**, 3306 (1994).
[42] P. Mendels, F. Bert, M. A. de Vries, A. Olariu, A. Harrison, F. Duc, J. C. Trombe, J. S. Lord, A. Amato, and C. Baines, Phys. Rev. Lett. **98**, 077204 (2007).
[43] J. S. Helton, K. Matan, M. P. Shores, E. A. Nytko, B. M. Bartlett, Y. Yoshida, Y. Takano, A. Suslov, Y. Qiu, J.-H. Chung, D. G. Nocera, and Y. S. Lee, Phys. Rev. Lett. **98**, 107204 (2007).
[44] O. Petrenko, C. Ritter, M. Yethiraj, and D. McK. Paul, Physica B **241-243**, 727 (1997).
[45] S. Nakatsuji, Y. Nambu, H. Tonomura, O. Sakai, S. Jonas, C. Broholm, H. Tsunetsugu, Y. Qiu, and Y. Maeno, Science **309**, 1697 (2005).
[46] Y. Shimizu, K. Miyagawa, K. Kanoda, M. Maesato, and G. Saito, Phys. Rev. Lett. **91**, 107001 (2003).
[47] I. Mirebeau, A. Apetrei, J. Rodríguez-Carvajal, P. Bonville, A. Forget, D. Colson, V. Glazkov, J. P. Sanchez, O. Isnard, and E. Suard, Phys. Rev. Lett. **94**, 246402 (2005).
[48] M. T. Hutchings, Solid State Phys. **16**, 1381 (1963).
[49] K. R. Lea, M. J. M. Leask, and W. P. Wolf, J. Phys. Chem. Solids **23**, 1381 (1962).
[50] P. Fabi, ISIS, Annual Report No. RAL-TR-95-023, 1995 (unpublished).
[51] H. A. Bethe, *Splitting of Terms in Crystals* (Consultants Bureau, New York, 1929); Complete English translation from Ann. Phys. **395**, 133 (1929).
[52] S. Nagata, H. Sasaki, K. Suzuki, J. Kiuchi, and N. Wada, J. Phys. Chem. Solids **62**, 1123 (2001).
[53] J. J. Smit, H. J. Van Wijk, L. J. De Jongh, and R. L. Carlin, Chem. Phys. Lett. **62**, 158 (1979).
[54] J.-M. Broto, H. Rakoto, and Z. A. Kazei, J. Phys.: Condens. Matter **15**, 8767 (2003).
[55] Z. A. Kazei, V. V. Snegirev, A. S. Andreenko, and O. D. Kondratiev, J. Magn. Magn. Mater. **300**, e430 (2006).
[56] J. H. V. Vleck, *The Theory of Electric and Magnetic Susceptibilities* (Oxford University Press, New York, 1932).
[57] J. Jensen and A. R. Mackintosh, *Rare Earth Magnetism* (Clarendon, Oxford, 1991).
[58] D. Bunbury, C. Carboni, and M. McCausland, J. Phys.: Condens. Matter **1**, 1309 (1989).
[59] B. Bleaney, Physica (Utrecht) **69**, 317 (1973).